United States Department of Commerce
Technology Administration
National Institute of Standards and Technology

NISTIR 5079

Dipole Moments of Weak, Electrically Small Emitters from TEM-Cell Measurements

David A. Hill
Kenneth H. Cavcey

NISTIR 5079

Dipole Measurements of Weak, Electrically Small Emitters from TEM-Cell Measurements

David A. Hill
Kenneth H. Cavcey

Radio-Frequency Technology Division
Electronics and Electrical Engineering Laboratory
National Institute of Standards and Technology
Boulder, Colorado 80303-3328

Through the Office of Law Enforcement Standards

Prepared for
National Institute of Justice
Office of Justice Programs
U.S. Department of Justice
Washington, DC 20531

December 1998

U.S. DEPARTMENT OF COMMERCE, William M. Daley, Secretary
TECHNOLOGY ADMINISTRATION, Gary R. Bachula, Acting Under Secretary for Technology
NATIONAL INSTITUTE OF STANDARDS AND TECHNOLOGY, Raymond G. Kammer, Director

National Institute of Justice

Jeremy Travis
Director

The technical effort to develop this standard was conducted under Interagency Agreement No. 94-IJ-R-004, Project No. 97-017CTT

This report was prepared by the Office of Law Enforcement Standards (OLES) of the National Institute of Standards and Technology (NIST) under the direction of A. George Lieberman, Program Manager for Communications Systems, and Kathleen M. Higgins, Director of OLES. The research resulting in this report was performed by David A. Hill and Kenneth H. Cavcey of the NIST Boulder laboratories, Electronics and Electrical Engineering Laboratory, Radio Frequency Technology Division. The work was sponsored by the National Institute of Justice, David G. Boyd, Director, Office of Science and Technology.

ABOUT THE LAW ENFORCEMENT AND CORRECTIONS STANDARDS AND TESTING PROGRAM

The Law Enforcement and Corrections Standards and Testing Program is sponsored by the Office of Science and Technology of the National Institute of Justice (NIJ), U.S. Department of Justice. The program responds to the mandate of the Justice System Improvement Act of 1979, which created NIJ and directed it to encourage research and development to improve the criminal justice system and to disseminate the results to Federal, State, and local agencies.

The Law Enforcement and Corrections Standards and Testing Program is an applied research effort that determines the technological needs of justice system agencies, sets minimum performance standards for specific devices, tests commercially available equipment against those standards, and disseminates the standards and the test results to criminal justice agencies nationally and internationally.

The program operates through:

The *Law Enforcement and Corrections Technology Advisory Council* (LECTAC) consisting of nationally recognized criminal justice practitioners from Federal, State, and local agencies, which assesses technological needs and sets priorities for research programs and items to be evaluated and tested.

The *Office of Law Enforcement Standards* (OLES) at the National Institute of Standards and Technology, which develops voluntary national performance standards for compliance testing to ensure that individual items of equipment are suitable for use by criminal justice agencies. The standards are based upon laboratory testing and evaluation of representative samples of each item of equipment to determine the key attributes, develop test methods, and establish minimum performance requirements for each essential attribute. In addition to the highly technical standards, OLES also produces technical reports and user guidelines that explain in nontechnical terms the capabilities of available equipment.

The *National Law Enforcement and Corrections Technology Center* (NLECTC), operated by a grantee, which supervises a national compliance testing program conducted by independent laboratories. The standards developed by OLES serve as performance benchmarks against which commercial equipment is measured. The facilities, personnel, and testing capabilities of the independent laboratories are evaluated by OLES prior to testing each item of equipment, and OLES helps the NLECTC staff review and analyze data. Test results are published in Equipment Performance Reports designed to help justice system procurement officials make informed purchasing decisions.

Publications are available at no charge from the National Law Enforcement and Corrections Technology Center. Some documents are also available online through the Internet/World Wide Web. To request a document or additional information, call 800-248-2742 or 301-519-5060, or write:

National Law Enforcement and Corrections Technology Center
P.O. Box 1160
Rockville, MD 20849-1160
E-mail: *asknlectc@nlectc.org*
World Wide Web address: *http://www.nlectc.org*

> The National Institute of Justice is a component of the Office of Justice Programs, which also includes the Bureau of Justice Assistance, Bureau of Justice Statistics, Office of Juvenile Justice and Delinquency Prevention, and the Office for Victims of Crime.

CONTENTS

FOREWORD

The Office of Law Enforcement Standards (OLES) of the National Institute of Standards and Technology (NIST) furnishes technical support to the National Institute of Justice (NIJ) program to strengthen law enforcement and criminal justice in the United States. OLES's function is to conduct research that will assist law enforcement and criminal justice agencies in the selection and procurement of quality equipment.

OLES is: (1) Subjecting existing equipment to laboratory testing and evaluation, and (2) conducting research leading to the development of several series of documents, including national standards, user guides, and technical reports.

This document covers research conducted by OLES under the sponsorship of the NIJ. Additional reports as well as other documents are being issued under the OLES program in the areas of protective clothing and equipment, communications systems, emergency equipment, investigative aids, security systems, vehicles, weapons, and analytical techniques and standard reference materials used by the forensic community.

Technical comments and suggestions concerning this report are invited from all interested parties. They may be addressed to the Office of Law Enforcement Standards, National Institute of Standards and Technology, Gaithersburg, MD 20899-8102.

David G. Boyd, Director
Office of Science and Technology
National Institute of Justice

PREFACE

This is the second report in a two-year project on Detection of Electronic Bomb Detonators, and it covers the period from January 1998 to October 1998. The project is sponsored by the National Institute of Justice, David G. Boyd, Director, Office of Science and Technology. The research was performed by the NIST Radio Frequency Technology Division and was monitored by A. George Lieberman, Program Manager for Communications Systems, and Kathleen M. Higgins, Director of the Office of Law Enforcement Standards (OLES).

The main topics addressed in this report are (1) the development of a new method for characterizing weak low-frequency emitters from measurements in TEM-cells and (2) the measured emissions from commercial electronic timers of the type that could be used in bomb detonators. The new TEM-cell measurement method is important because it satisfies the need to provide a simple, quantitative method for characterizing low-frequency electric and magnetic field emissions from electronic timers. The method has higher sensitivity than previous methods, and we have been able to measure low-frequency, electric-dipole emissions from two commercial electronic timers. The magnetic-dipole radiation was found to be below the noise floor of the measurement system. The radiated power was found to be too low to attempt far-field detection from radiated fields.

The practical implication of these TEM-cell measurements on commercial electronic timers is that they do radiate low-frequency electric fields that can be detected in a sensitive TEM cell. Such a device could be used for inspection of luggage that would be passed through the cell, but a portable detection system that could be used to inspect a site would be more desirable. The results in this report indicate that future work should include a feasibility study of near-field, dipole-antenna arrays for detection of low-frequency, electric-field emissions from electronic timers. The main question to be answered is what is the range of a portable dipole array for detecting weak, electric-dipole fields in a real-world, noisy environment.

The first report on this project covered the theory of separating the fields of interest (from electronic timers) from undesired noise fields from external sources by using the techniques of spherical, near-field scanning as developed at NIST:

Hill, D.A. Spherical-wave characterization of interior and exterior electromagnetic sources. Natl. Inst. Stand. Technol. NISTIR 5072; December 1997.

DIPOLE MOMENTS OF WEAK, ELECTRICALLY SMALL EMITTERS FROM TEM-CELL MEASUREMENTS

David A. Hill and Kenneth H. Cavcey

Radio Frequency Technology Division
National Institute of Standards and Technology
Boulder, Colorado 80303

This report presents a new method for determining the equivalent electric and magnetic dipole moments of an electrically small emitter from TEM-cell measurements. The electric dipole moments are determined from open-circuit measurements, and the magnetic dipole moments are determined from short-circuit measurements. The method has the advantages of simplicity in separating the electric and magnetic dipole emissions and increased sensitivity resulting from the in-phase reflection from the open- or short-circuited port. The method has been used on two commercial electronic timers, and in both cases the electric dipole moment was measurable, but the magnetic dipole response was below the noise floor. These results have practical application to the problem of detection of electronic bomb detonators.

Key words: capacitance; dipole moment; electrically small emitter; electric dipole; inductance; magnetic dipole; quasi-static fields; reciprocity; TEM cell.

1. INTRODUCTION

Electrically small emitters (with dimensions much less than a free-space wavelength) can be characterized by their electric and magnetic dipole moments. Measurement of these dipole moments could be viewed as a special case of spherical, near-field scanning [1] with only six unknowns (three orthogonal electric and three orthogonal magnetic dipole moments) to be determined [2]. Specialized measurement methods using three orthogonal loop antennas [3] or both ports of a transverse electromagnetic (TEM) cell [4] have also been implemented.

The purpose of this report is to present a new TEM-cell measurement method that uses an open-circuited cell to determine electric dipole moments or a short-circuited cell to determine magnetic dipole moments. This method has a smaller bandwidth than the earlier TEM-cell method [4], but it is more sensitive. The increased sensitivity has been found useful in measuring weak, low-frequency emissions from electronic timers of the type that could be used in a bomb detonator.

2. RECIPROCITY THEORY FOR A TEM CELL

TEM cells [5] have been used extensively in electromagnetic compatibility (EMC) measurements because they provide a shielded environment and have no low-frequency cutoff. They typically have a uniform section of rectangular coaxial transmission line tapered at each end to adapt to standard coaxial connectors as shown in figure 1. The uniform center section and tapered transitions usually have a characteristic impedance of 50 Ω along their entire length.

A cross section of the center uniform section of the cell is shown in figure 2. The equipment under test (EUT) is placed on the centerline (y axis) to take advantage of the cell symmetry. The cell is assumed to be symmetrical about both the xz and yz planes. Only the TEM mode is considered in this analysis; so the frequency of operation must be below the cutoff frequencies of all higher-order modes [6],[7].

Excitation of a TEM cell by an electrically small EUT is best analyzed using reciprocity theory [8], and an analysis for general terminations of the two ports is presented in the Appendix. However, our measurement configuration uses either an open or short circuit at one end with a detector at the opposite end. These simpler configurations are easier to analyze and provide more physical insight; so they will be analyzed in detail in this section.

2.1 Electric-Dipole Excitation of an Open-Circuited Cell

A side view of an open-circuited TEM cell is shown in figure 3. The opposite port is terminated with an impedance Z_l which is arbitrary at this point. The surface S coincides with the interior boundary of the cell and also crosses the coaxial transmission lines at both ports. Reciprocity theory requires two field states which we denote states 1 and 2. The electric and magnetic fields, $\boldsymbol{E}_1$ and $\boldsymbol{H}_1$, of state 1 are generated by a voltage source at the right-hand termination. The electric and magnetic fields, $\boldsymbol{E}_2$ and $\boldsymbol{H}_2$, are generated by electric and magnetic currents, $\boldsymbol{J}_2$ and $\boldsymbol{M}_2$, in the EUT. A general reciprocity relationship involving both surface (S) and volume (V) integrals can be written [8]

$$\iint_S [\boldsymbol{E}_1(\boldsymbol{r}) \times \boldsymbol{H}_2(\boldsymbol{r}) - \boldsymbol{E}_2(\boldsymbol{r}) \times \boldsymbol{H}_1(\boldsymbol{r})] \bullet \hat{\boldsymbol{n}}\, \mathrm{d}S = -\iiint_V [\boldsymbol{J}_2(\boldsymbol{r}) \bullet \boldsymbol{E}_1(\boldsymbol{r}) - \boldsymbol{M}_2(\boldsymbol{r}) \bullet \boldsymbol{H}_1(\boldsymbol{r})]\, \mathrm{d}V, \tag{1}$$

where $\hat{\boldsymbol{n}}$ is the outward unit normal to the surface S. The time dependence of the fields and currents is $\exp(j\omega t)$. Since the cell is open circuited and the length L is much smaller than the free-space wavelength λ, the reflection from the open circuit doubles the electric field in the test volume due to the voltage source (state 1) and cancels the magnetic field in the test volume. So the second term on the right side of eq (1) vanishes.

For an electrically small EUT located as indicated in figure 3, the electric current $\boldsymbol{J}_2$ can be approximated

$$\boldsymbol{J}_2(\boldsymbol{r}) = [\hat{x} d_{ex} + \hat{y} d_{ey} + \hat{z} d_{ez}]\, \delta(x)\delta(y - y_1)\delta(z), \tag{2}$$

where d_{ex}, d_{ey}, and d_{ez} are x-, y-, and z-directed current moments, δ is the Dirac delta function, and y_1 is the center height of the EUT above the septum. We use the term current moment because d_{ex}, d_{ey}, and d_{ez} have dimensions of current times length (A•m). (We will later use the term dipole moment for charge times length.) The electric field on the centerline of the test zone ($x = z = 0$) can be approximated

$$\boldsymbol{E}_1(\hat{y}y) = \hat{y}V_1 / h, \tag{3}$$

where h is the separation between the septum and the outer conductor and V_1 is the voltage between the two conductors. Equation (3) is only an approximation, and more accurate expressions and numerical results for the y dependence are available [9], [10]. The actual electric field strength is larger near the septum and smaller near the outer conductor, but we use eq (3) because the center of the EUT is located somewhat above the septum where eq (3) is an adequate approximation. The right side of eq (1) can now be evaluated from eqs (2) and (3) and the sampling property of the delta function:

$$-\iiint_V \boldsymbol{J}_2(\boldsymbol{r}) \bullet \boldsymbol{E}_1(\boldsymbol{r})\, \mathrm{d}V = -\frac{d_{ey}V_1}{h}. \tag{4}$$

Consider now the evaluation of the surface integral on the left side of eq (1). The integrand is zero on the conducting surface (assumed to be perfectly conducting) because the tangential components of electric fields, $\boldsymbol{E}_1$ and $\boldsymbol{E}_2$, are zero. The integrand is zero on the surface of the open-circuit port because the tangential components of the magnetic fields, $\boldsymbol{H}_1$ and $\boldsymbol{H}_2$, are zero. This leaves only the port that is terminated in impedance Z_l to contribute to the integral. Figure 4 shows the surface S at the terminated port in detail. The port is a circularly symmetric coaxial transmission line with inner radius a and outer radius b. Only the portion of the surface S between the two conductors contributes to the integral, and we follow the evaluation method of Monteath [8]. The electric field $\boldsymbol{E}_1$ has only a radial component E_{1r} which can be written

$$E_{1r}(r) = \frac{V_1}{r \ln(b/a)}, \quad a \le r \le b, \tag{5}$$

where r is the radial coordinate. The magnetic field $\boldsymbol{H}_2$ has only an azimuthal component $H_{2\phi}$ which can be written

$$H_{2\phi}(r) = \frac{I_2}{2\pi r}, \quad a \le r \le b. \tag{6}$$

We can now evaluate the first term in eq (1) by using eqs (5) and (6):

$$\iint_S \boldsymbol{E}_1(\boldsymbol{r}) \times \boldsymbol{H}_2(\boldsymbol{r}) \bullet \hat{\boldsymbol{n}}\, \mathrm{d}S = \int_a^b \frac{V_1}{r \ln(b/a)} \frac{I_2}{2\pi r} 2\pi r\, \mathrm{d}r = V_1 I_2. \tag{7}$$

The evaluation of the second term in eq (1) is the same except that the subscripts 1 and 2 are interchanged.

Using eqs (4) and (7), we can now write eq (1) in the following form:

$$V_1 I_2 - V_2 I_1 = -\frac{d_{ey} V_1}{h}. \tag{8}$$

Equation (8) is essentially a circuit version of eq (1), and it can be cast in a more useful form by eliminating the currents I_2 and I_1. Since the cell is terminated in an impedance Z_l, we can replace I_2 by

$$I_2 = V_2 / Z_l. \tag{9}$$

The electrically short, open-circuit cell acts like a capacitor of capacitance C_L. We use the subscript L because the capacitance can be written as the product of the cell length L and the capacitance per unit length [5]:

$$C_L = L \frac{1}{c Z_0}, \tag{10}$$

where c is the velocity of light and Z_0 is the characteristic impedance of the cell (usually 50 Ω). (We assume that the characteristic impedance of the center section is maintained in the tapered sections.) The current I_1 can be written as the product of the voltage V_1 and the cell admittance:

$$I_1 = -j\omega C_L V_1, \tag{11}$$

where we assume a time dependence $\exp(j\omega t)$. The minus sign in eq (11) arises from the convention of the current and voltage as shown in figure 4. If we substitute eqs (9) and (11) in eq (8), we obtain our desired result relating d_{ey} and V_2:

$$-\frac{d_{ey}}{h} = V_2 \left(j\omega C_L + \frac{1}{Z_l} \right). \tag{12}$$

Since h and C_L are known properties of the cell, the current moment d_{ey} can be determined from a measurement of the voltage V_2 across the load impedance Z_l. Equation (12) has a simple equivalent circuit interpretation as shown in figure 5. The current source is equal to $-d_{ey}/h$, and the cell capacitance and load impedance form a parallel circuit. Measurements with three orthogonal orientations of the EUT will determine the three orthogonal current moments.

2.2 Magnetic-Dipole Excitation of a Short-Circuited Cell

The geometry analyzed in this section is shown in figure 6. It is the same as figure 3 except that the cell is short circuited instead of open circuited. Our starting point is again the general reciprocity relationship in eq (1). In this case the reflection from the short circuit doubles the magnetic field in the test volume due to the voltage source (state 1) and cancels the electric field in the test volume. So the first term on the right side of eq (1) vanishes.

The magnetic current M_2 of the EUT can be approximated as

$$M_2(r) = [\hat{x}d_{mx} + \hat{y}d_{my} + \hat{z}d_{mz}]\delta(x)\delta(y - y_1)\delta(z), \tag{13}$$

where d_{mx}, d_{my}, and d_{mz} are x-, y-, and z-directed magnetic current moments. Since the dominant field in the cell is a TEM mode, the magnetic field on the centerline is related to the electric field in eq (3) by the reciprocal of the free-space impedance η:

$$H_1(\hat{y}y) = -\hat{x}\frac{V_1}{h\eta}. \tag{14}$$

In this case the right side of eq (1) can be evaluated from eqs (13) and (14):

$$\iiint_V M_2(r) \bullet H_1(r) \mathrm{d}V = -\frac{d_{mx}V_1}{\eta h}. \tag{15}$$

The evaluation of the surface integrals in eq (1) is similar to that in the previous section. This time the integrand is zero on the surface of the short-circuited port because the tangential components of the electric fields, E_1 and E_2, are zero. The evaluation of the surface integral at the terminated port in terms of voltages and currents follows the same procedure as in eq (7). So eq (1) reduces to

$$V_1 I_2 - I_1 V_2 = -\frac{d_{mx}V_1}{\eta h}. \tag{16}$$

The electrically short, short-circuit cell acts like an inductor of inductance L_L. We use the subscript L because the inductance can be written as the product of the cell length L and the inductance per unit length:

$$L_L = L\frac{Z_0}{c}. \tag{17}$$

Equations (10) and (17) satisfy the following consistency check from transmission line theory [11]:

$$\sqrt{\frac{L_L}{C_L}} = Z_0. \tag{18}$$

The voltage V_1 can be written as the current I_1 times the cell impedance:

$$V_1 = -j\omega L_L I_1, \tag{19}$$

where the minus sign is a result of the current and voltage convention in figure 4. If we make use of eqs (9) and (19) and the characteristic impedance Z_0 of the cell, we can write eq (16) in the following form relating d_{mx} and V_2:

$$V_2 = \frac{d_{mx} Z_0}{h\eta} \frac{Z_l}{j\omega L_L + Z_l}. \tag{20}$$

Equation (20) can be used to determine the magnetic current moment d_{mx} from a measurement of the voltage V_2 across the load impedance Z_l. Equation (20) also has a simple equivalent circuit interpretation as shown in figure 7. The voltage source is equal to $d_{mx}Z_0/(h\eta)$, and the cell inductance and load impedance form a series circuit. Measurements with three orthogonal orientations of the EUT will determine the three orthogonal magnetic current moments.

3. TEM-CELL MEASUREMENTS

3.1 Measurement Method

The measurement configurations with an open-circuited TEM cell shown in figure 3 and with a short-circuited TEM cell shown in figure 6 were implemented with the same TEM cell. The cell length L is 73.0 cm, and the cell half height h is 14.8 cm. The cell and septum widths do not appear directly in the measurement theory, but they are chosen [5] so that the characteristic impedance Z_0 of the cell is 50 Ω. Since the cell must be electrically short ($L/\lambda < 0.1$), the upper frequency limit for this cell of 73.0 cm is approximately 40 MHz. For small test objects, the cell could be shortened to raise the upper frequency limit.

Calculated from eq (10), the open-circuit cell capacitance $C_L = 48.7$ pF. We measured a value of 53.2 pF. From eq (17), the calculated short-circuit cell inductance $L_L = 0.122$ μH. We measured a value of 0.184 μH. We used a large resistive load impedance $Z_l = 10$ MΩ.

Because of the large value of Z_l, eq (12) simplifies to the following for frequencies of interest (> 100 kHz):

$$d_{ey} \approx -j\omega C_L h V_2. \tag{21}$$

Equation 21 is a useful expression for the current moment d_{ey}, but for later field calculations we prefer to use the dipole moment p_{ey} which is given by [12]

$$p_{ey} = \frac{d_{ey}}{j\omega} \approx -C_L h V_2. \tag{22}$$

The dipole moment has dimensions of charge-length or units of C•m.

Because of the large value of Z_l, eq (20) can also be simplified to

$$d_{mx} \approx \frac{h\eta V_2}{Z_0}. \tag{23}$$

It is fortunate that this result does not depend on the short-circuit cell inductance L_L since the calculated and measured values of L_L do not agree well. All that is required for the validity of eq

(23) is that $Z_l >> \omega L_L$. The magnetic dipole moment p_{mx} can be determined from the magnetic current moment in eq (23) by [12]

$$p_{mx} = \frac{d_{mx}}{j\omega} \approx \frac{h\eta V_2}{j\omega Z_0}. \tag{24}$$

The magnetic dipole moment has dimensions of magnetic charge times length or units of C•Ω•m.

Measurements were performed on two small electronic timers of the type that could be used in bomb detonators. A photograph of the smaller timer inside the TEM cell (with the access door open) is shown in figure 8. A closeup on the smaller timer on the septum is shown in figure 9. The other timer is similar, but somewhat larger. The dimensions of the smaller timer are 5.21 cm × 5.50 cm × 0.85 cm, and the dimensions of the larger timer are 6.05 cm × 6.05 cm × 0.85 cm. These timers are very weak emitters, and a 50 dB amplifier was used following the load impedance to raise the signal to levels that were measurable. The amplifier matched the high load impedance (10 MΩ) to 50 Ω. The frequency spectrum was then measured with a spectrum analyzer, and the time-domain waveform was measured with an oscilloscope.

We also attempted to use the sum-and-difference method with the two outputs of the same cell for simultaneously determining one electric dipole moment and one magnetic dipole moment [4]. However, we found that this method did not have adequate sensitivity for measuring the weak emissions from the timers.

3.2 Measurement Results for Dipole Moments

Equation (22) relates the measured load voltage V_2 to the electric dipole moment p_{ey} when the opposite port is open circuited. We measured the magnitude of V_2 with a spectrum analyzer at 12 frequencies from 200 kHz to 8 MHz using a bandwidth of 100 kHz at each frequency. The three electric dipole moments of the larger timer were obtained from three orthogonal orientations of the timer. The height of the timer center was maintained at half of the timer width or height (approximately 3.03 cm) for all three orientations. The results for the magnitudes of the three dipole magnitudes in fC•m are given in table 1. These are small dipole moments since 1 femtocoulomb (fC) equals 10^{-15} coulomb (C). However, the quasi-static electric fields radiated by these dipole moments provide a more significant measure of the detectability of the emissions, and those results are given in the next section. A similar set of measurements was made on the smaller timer, and the resultant dipole moments had a similar frequency dependence, but were slightly smaller in magnitude.

We also used an oscilloscope to measure the corresponding time-domain waveform of V_2 with the opposite port open circuited. The waveform of V_2 was composed of a series of narrow pulses with peak amplitude of approximately 1mV. The waveform was periodic with a period of approximately 31 ms. This means that the spectrum consists of spectral lines separated by approximately 32 Hz. This is consistent with spectrum analyzer results, but we did not attempt to resolve the individual lines. Since the coefficient of V_2 in eq (22) is frequency independent, the dipole moment p_{ey} has the same time and frequency characteristics as V_2. An example of the time-domain waveform of the radiated electric field is given in the following section.

Equation (24) relates the measured load voltage V_2 to the magnetic dipole moment p_{mx} when the opposite port is short circuited. We attempted to measure V_2 with a spectrum analyzer over the same frequency range of 200 kHz to 8 MHz, but were not able to detect a signal at any frequency for any timer orientation. The noise floor for V_2 was approximately 11.5 μV (for the same 100 kHz bandwidth). Hence the signal has to be somewhat below that. So all that we can obtain from eq (24) is an upper bound on the magnetic dipole moment:

$$|p_{mx}| < \frac{h\eta V_{2n}}{\omega Z_0}, \tag{25}$$

where V_{2n} is the noise floor voltage across the load voltage. For example, at a frequency of 1 MHz and a noise floor voltage of 11.5 μV, the upper bound of $|p_{mx}|$ is 2.04×10^{-12} C•Ω•m. The resultant upper bound of the radiated magnetic field is discussed in the following section.

The results measured by the TEM-cell method described here are consistent with earlier NIST measurements on similar electronic timers. In both cases the near-field, electric-dipole radiation was measurable, but no near-field, magnetic-dipole radiation could be detected. The physical explanation is probably that there is sufficient charge separation to create detectable electric dipole moments in the circuitry or liquid crystal display. However, there are no current loops that are large enough to create measurable magnetic dipole moments.

4. DIPOLE RADIATION IN FREE SPACE

Once the dipole moments of an electrically small emitter are measured in a TEM cell, we can calculate the free-space radiated fields [13]. The assumption in doing the calculations is that the dipole moments remain the same in either a TEM-cell environment or a free-space environment.

4.1 Quasi-Static Fields

Because of the low frequencies (below 10 MHz) and weak radiation emitted by electronic timers, only the quasi-static near fields offer any possibility of detection with free-space field measurements. For quasi-static electric fields radiated by electric dipoles, the longitudinal field has twice the magnitude of the transverse field. For example, the radial electric field radiated off the end of a z-directed electric dipole is given by [13]

$$E_r\,|_{\theta=0} = \frac{p_{ez}}{2\pi\varepsilon_0 r^3}, \tag{26}$$

where ε_0 is the permittivity of free space and r and θ are standard spherical coordinates. Equation (26) is valid for $r/\lambda << 1$, and the radial electric field on the z axis is seen to be independent of the x- and y-directed electric dipole moments. Since the electric field is frequency independent, eq (26) is called the quasi-static result. Similar expressions can be written for the radial electric fields on the x and y axes as shown in figure 10:

$$E_r\,|_{\theta=\pi/2,\phi=0} = \frac{p_{ex}}{2\pi\varepsilon_0 r^3} \quad \text{and} \quad E_r\,|_{\theta=\phi=\pi/2} = \frac{p_{ey}}{2\pi\varepsilon_0 r^3}, \tag{27}$$

where ϕ is the azimuthal angle. The results in eqs (26) and (27) are consistent with the results for determining the dipole moments from radial field measurements given in [2].

Equations (26) and (27) can be used to determine the quasi-static electric fields on the three axes from the three electric dipole moments. For example, the three electric dipole moments of the larger electronic timer were given in table 1, and we have used that measured data to calculate electric field strength at distance r of 1 m as shown in table 2. The tabulated field strengths can be extrapolated to other distances by the inverse distance-cubed relationship in eqs (26) and (27). Since the three dipole moments are of similar magnitudes, the field strengths on the three axes are also of similar magnitudes. This result means that the direction or orientation of a sensing antenna is not critical to the detection of the source. The electric field strengths in table 2 drop with frequency so that the lower frequencies offer the most promise for detection. The other timer has similar radiation characteristics, but at a somewhat lower level.

Since the coefficients of the dipole moments in eqs (26) and (27) are frequency independent, they can also be used to obtain the time-domain fields from the time-domain waveforms of the dipole moments. Figure 11 shows a representative waveform for the radial field at a 1 m distance on the z axis. The maximum pulse height is seen to be about 1.4 mV/m, and the pulses are separated by about 4 ms. The fundamental period is approximately 31 ms. The field waveforms on the x and y axes have pulses in the same time locations, but have slightly different magnitudes. The smaller timer has similar radiated waveforms.

By duality, the radial quasi-static magnetic fields H_r on the three axes have the same form as eqs (26) and (27) except that the free-space permittivity is replaced by the free-space permeability μ_0:

$$H_r\,|_{\theta=\pi/2,\phi=0} = \frac{p_{mx}}{2\pi\mu_0 r^3}, \quad H_r\,|_{\theta=\phi=\pi/2} = \frac{p_{my}}{2\pi\mu_0 r^3}, \quad \text{and} \quad H_r\,|_{\theta=0} = \frac{p_{mz}}{2\pi\mu_0 r^3}. \tag{28}$$

Since we were not able to measure any magnetic dipole moments above the noise floor, we cannot use eq (28) to calculate magnetic field strength. However, we can use eq (28) to calculate an upper bound on the magnetic field strength. Table 3 shows the upper bound on the radial magnetic field as a function of frequency. The magnitudes are less than 1 μA/m.

4.2 Radiated Power

The power radiated by electronic timers is extremely small, but it is still interesting to quantify it. The total radiated power P_t can be written as the sum of the powers radiated by the electric and magnetic dipole moments [1]

$$P_t = P_e + P_m, \tag{29}$$

where

$$P_e = \frac{\eta \omega^4}{6\pi c^2}\left(|p_{ex}|^2 + |p_{ey}|^2 + |p_{ez}|^2\right), \tag{30}$$

$$P_m = \frac{\omega^4}{6\pi \eta c^2}\left(|p_{mx}|^2 + |p_{my}|^2 + |p_{mz}|^2\right), \tag{31}$$

and c is the speed of light in free space. The radiated power approaches zero at low frequencies because of the ω^4 factor.

The power radiated by the electric dipole moments can be calculated from eq (30) and the electric dipole moments in table 1. For example at 1 MHz, $P_e = 1.69 \times 10^{-17}$ W. This is actually the value in a 100 kHz bandwidth. The frequency dependence is fairly weak because the dipole moments decrease with frequency, but eqs (30) and (31) include an ω^4 coefficient. This extremely small radiated power offers very little hope of detecting the radiated fields in the far zone.

Since we have only an upper bound on the magnetic dipole moment, we can calculate only an upper bound on P_m from eq (31). For example at 1 MHz, $P_m < 10^{-17}$ W, which is less than P_e.

5. CONCLUSIONS

The theory and measurement technique have been developed for characterizing weak, low-frequency emitters with open-circuit and short-circuit TEM-cell measurements. The method is simpler and more direct than previous methods because the equivalent electric dipole moment is determined solely from open-circuit measurements and the equivalent magnetic dipole moment is determined solely from short-circuit measurements. The method is also more sensitive because it takes advantage of the in-phase reflection from the open or short circuit. The main disadvantage of this method is a smaller frequency range because the cell must be short compared to the wavelength. For the 0.73 m cell which was used here, the upper frequency limit is approximately 40 MHz.

The method was used on two commercial electronic timers of the type that could be used in a bomb detonator. Both timers generated three orthogonal electric dipole moments that were easily measured in both the time and frequency domains. However, magnetic dipole radiation was too weak to measure. The practical outcome of these measurements is that a detection method for electronic timers should be based on the quasi-static electric field at short ranges. This conclusion is consistent with past NIST measurements on similar timers. The expected electric field strength at distances greater than 1 m is somewhat less than 1mV/m as shown in table 2.

A useful extension of this work would be to measure the weak electric fields of electronic timers with a dipole array. A method for canceling the competing fields from noise sources has been analyzed in [2]. The measurement uncertainty of this TEM-cell method needs to be determined. Well established TEM cell measurements [5] have been shown to have measurement uncertainties of approximately 0.8 dB; so this newly developed method probably has an expanded uncertainty (with a coverage factor of 2) of approximately 1.5 dB. It would also be useful to perform measurements with a known calibrated source [14] in the TEM cell.

REFERENCES

[1] Hansen, J.E., editor. *Spherical Near-Field Antenna Measurements*. London: Peter Perigrinus; 1988.

[2] Hill, D.A. Spherical-wave characterization of interior and exterior electromagnetic sources. Natl. Inst. Stand. Technol. Interagency Report 5072; 1997.

[3] Kanda, M.; Hill, D.A. A three-loop system for determining the radiation characteristics of an electrically small source. *IEEE Trans. Electromag. Compat., 34*: 1-3; 1992.

[4] Sreenivasiah, I.; Chang, D.C.; Ma, M.T. Emission characteristics of electrically small radiating sources from tests inside a TEM cell. *IEEE Trans. Electromag. Compat., 23*: 113-121; 1981.

[5] Kanda, M.; Orr, R.D. Generation of standard electromagnetic fields in a TEM cell. Nat. Bur. Stand. (U.S.) Technical Note 1319; 1988.

[6] Hill, D.A. Bandwidth limitations of TEM cells due to resonances. *J. Microwave Power, 18*: 181-195; 1983.

[7] Wilson, P.F.; Ma, M.T. Simple approximate expressions for higher order mode cutoff and resonant frequencies in TEM cells. *IEEE Trans. Electromag. Compat., 28*: 125-130; 1986.

[8] Monteath, G.D. *Applications of the Electromagnetic Reciprocity Principle*. Oxford: Pergamon Press; 1973.

[9] Tippet, J.C.; Chang, D.C. Radiation characteristics of dipole sources located inside a rectangular, coaxial transmission line. Nat. Bur. Stand. (U.S.) Interagency Report 75-829; 1976.

[10] Wilson, P. On correlating TEM cell and OATS emission measurements. *IEEE Trans. Electromag. Compat., 37*: 1-16; 1995.

[11] Johnson, W.C. *Transmission Lines and Networks*. New York: McGraw-Hill; 1950.

[12] Stratton, J.A. *Electromagnetic Theory*. New York: McGraw-Hill; 1941.

[13] Harrington, R.F. *Time-Harmonic Electromagnetic Fields*. New York: McGraw-Hill; 1961.

[14] Koepke, G.; Randa, J. Screened-room measurements on the NIST spherical-dipole standard radiator. *J. Res. Natl. Inst. Stand. Technol., 99*: 737-749; 1994.

APPENDIX: TEM-CELL THEORY FOR ARBITRARY TERMINATIONS

In this appendix, we generalize the theory in Section 2 to allow arbitrary terminations at both ports of the TEM cell and to account for arbitrary electrical length of the cell. The geometry shown in figure 12 is the same as in figures 3 and 6 except that the termination at $z = -L/2$ is an arbtrary impedance Z_t.

We divide the cell into region 1 (for negative z) and region 2 (for positive z). The fields in each region consist of TEM modes traveling in the positive and negative z directions. In region 1, we write the electric $\boldsymbol{E}_1$ and magnetic $\boldsymbol{H}_1$ fields as

$$\boldsymbol{E}_1 = a_1 \boldsymbol{E}_0^+ + b_1 \boldsymbol{E}_0^- \quad \text{and} \quad \boldsymbol{H}_1 = a_1 \boldsymbol{H}_0^+ + b_1 \boldsymbol{H}_0^- . \tag{A1}$$

Similarly, in region 2 we write the electric $\boldsymbol{E}_2$ and magnetic $\boldsymbol{H}_2$ fields as

$$\boldsymbol{E}_2 = a_2 \boldsymbol{E}_0^+ + b_2 \boldsymbol{E}_0^- \quad \text{and} \quad \boldsymbol{H}_2 = a_2 \boldsymbol{H}_0^+ + b_2 \boldsymbol{H}_0^- . \tag{A2}$$

The TEM-cell modes traveling in the positive and negative z directions can be written

$$\boldsymbol{E}_0^{\pm} = (\hat{x} e_{0x} + \hat{y} e_{0y}) \exp(\mp jkz) \quad \text{and} \quad \boldsymbol{H}_0^{\pm} = \pm \frac{1}{\eta} \hat{z} \times \boldsymbol{E}_0^{\pm} , \tag{A3}$$

where the modes are normalized to carry a power of 1 W.

The four unknown coefficients, a_1, b_1, a_2, and b_2, are determined from the source conditions of the EUT and the termination conditions. The EUT source conditions at $z = 0$ are determined from reciprocity, and they can be written [4]

$$a_2 - a_1 = \frac{1}{2}\left(-d_{ey} e_{0y} + d_{mx} \frac{e_{0y}}{\eta} \right) \tag{A4}$$

and

$$b_1 - b_2 = -\frac{1}{2}\left(d_{ey} e_{0y} + d_{mx} \frac{e_{0y}}{\eta} \right). \tag{A5}$$

The termination condition at $z = -L/2$ can be written

$$a_1 \exp\left(jk \frac{L}{2} \right) = R_t b_1 \exp\left(-jk \frac{L}{2} \right), \quad \text{where} \quad R_t = \frac{Z_t - Z_0}{Z_t + Z_0}. \tag{A6}$$

The termination condition at $z = L/2$ can be written

$$b_2 \exp\left(jk \frac{L}{2} \right) = R_l a_2 \exp\left(-jk \frac{L}{2} \right), \quad \text{where} \quad R_l = \frac{Z_l - Z_0}{Z_l + Z_0}. \tag{A7}$$

Simultaneous solution of eqs (A4) through (A7) yields

$$a_1 = -R_t \exp(-jkL) \frac{d_{ey} e_{0y} [1 + R_l \exp(-jkL)] + d_{mx} \dfrac{e_{0y}}{\eta} [1 - R_l \exp(-jkL)]}{2[1 - R_l R_t \exp(-j2kL)]}, \qquad \text{(A8)}$$

$$a_2 = \frac{-d_{ey} e_{0y} [1 - R_t \exp(-jkL)] + d_{mx} \dfrac{e_{0y}}{\eta} [1 - R_t \exp(-jkL)]}{2[1 - R_l R_t \exp(-j2kL)]}, \qquad \text{(A9)}$$

$$b_1 = -\frac{d_{ey} e_{0y} [1 + R_l \exp(-jkL)] + d_{my} \dfrac{e_{0y}}{\eta} [1 - R_l \exp(-jkL)]}{2[1 - R_l R_t \exp(-j2kL)]}, \qquad \text{(A10)}$$

$$b_2 = R_l \exp(-jkL) \frac{-d_{ey} e_{0y} [1 + R_t \exp(-jkL)] + d_{mx} \dfrac{e_{0y}}{\eta} [1 - R_t \exp(-jkL)]}{2[1 - R_l R_t \exp(-j2kL)]}. \qquad \text{(A11)}$$

Now that the mode coefficients are known, we can determine the fields in the cell or the termination voltages or currents. The quantity of most practical interest is the voltage V_2 across the load impedance Z_l. We assume that the taper of the cell does not affect this result because the characteristic impedance Z_0 is maintained throughout the entire length L. We also make the approximation that the electric field e_{0y} of the TEM mode is approximately uniform in the y direction on the y axis. With the power normalization given earlier, e_{0y} can be approximated

$$e_{0y} \approx \sqrt{Z_0} / h. \qquad \text{(A12)}$$

Now V_2 can be written

$$V_2 \approx h\hat{\mathbf{y}} \bullet \mathbf{E}_2 |_{z=L/2, x=0} \qquad \text{(A13)}$$

$$\approx Z_0 (1 + R_l) \exp\left(-jk\frac{L}{2}\right) \frac{-d_{ey} [1 + R_t \exp(-jkL)] + \dfrac{d_{mx}}{\eta} [1 - R_t \exp(-jkL)]}{2h[1 - R_l R_t \exp(-j2kL)]}.$$

To this point, we have imposed no restriction on L. If we wish to study the low-frequency behavior of V_2, we can replace the exponentials in the field or voltage equation by the small argument approximation:

$$\exp(-jkL) \approx 1 - jkL. \qquad \text{(A14)}$$

Consider now the open-circuit case, $R_t = 1$. If we substitute 1 for R_t and use the small-argument approximations for the exponentials, eq (A13) reduces to

$$V_2 \approx \frac{-d_{ey}/h}{j\omega C_L + \dfrac{1}{Z_l}}. \tag{A15}$$

This result is equivalent to eq (12) which was derived by starting with low-frequency approximations.

For the short-circuit case, we have $R_t = -1$. Using this result plus the small-argument approximations for the exponentials in eq (A13), we can obtain

$$V_2 \approx \frac{d_{mx} Z_0}{h\eta} \frac{Z_l}{Z_l + j\omega L_L}. \tag{A16}$$

This result is identical to eq (20) which was derived by starting with low-frequency approximations.

Table 1. Measured electric dipole moments versus frequency.

Frequency (MHz)	$\lvert p_{ex} \rvert$ (fC•m)	$\lvert p_{ey} \rvert$ (fC•m)	$\lvert p_{ez} \rvert$ (fC•m)
0.2	23.1	20.5	25.2
0.3	15.8	11.4	16.3
0.5	9.50	7.21	8.18
0.7	6.96	5.28	6.28
1.0	4.40	3.78	3.92
2.0	2.11	1.92	1.96
3.0	1.24	1.16	1.30
4.0	0.928	0.876	0.828
5.0	0.635	0.642	0.628
6.0	0.572	0.440	0.440
7.0	0.370	0.329	0.301
8.0	0.280	0.252	0.231

Table 2. Radial electric field strength at 1 m from electronic timer.

Frequency	$\lvert E_r \rvert$ (on x axis)	$\lvert E_r \rvert$ (on y axis)	$\lvert E_r \rvert$ (on z axis)
0.2 MHz	415.0 μV/m	369.0 μV/m	454.0 μV/m
0.3	284.0	205.0	293.0
0.5	170.8	129.6	147.1
0.7	125.2	95.0	112.9
1.0	79.1	67.9	70.4
2.0	37.8	34.5	35.3
3.0	22.3	20.8	23.3
4.0	16.7	15.8	14.9
5.0	11.4	11.6	11.3
6.0	10.3	7.91	7.91
7.0	6.65	5.92	5.40
8.0	5.04	4.54	4.15

Table 3. Upper bound of radial magnetic field at 1 m from electronic timer.

Frequency (MHz)	$\lvert H_r \rvert$ (μA/m)
0.2	1.29
0.3	0.860
0.5	0.516
0.7	0.369
1.0	0.258
2.0	0.129
3.0	0.0860
4.0	0.0645
5.0	0.0516
6.0	0.0430
7.0	0.0368
8.0	0.0323

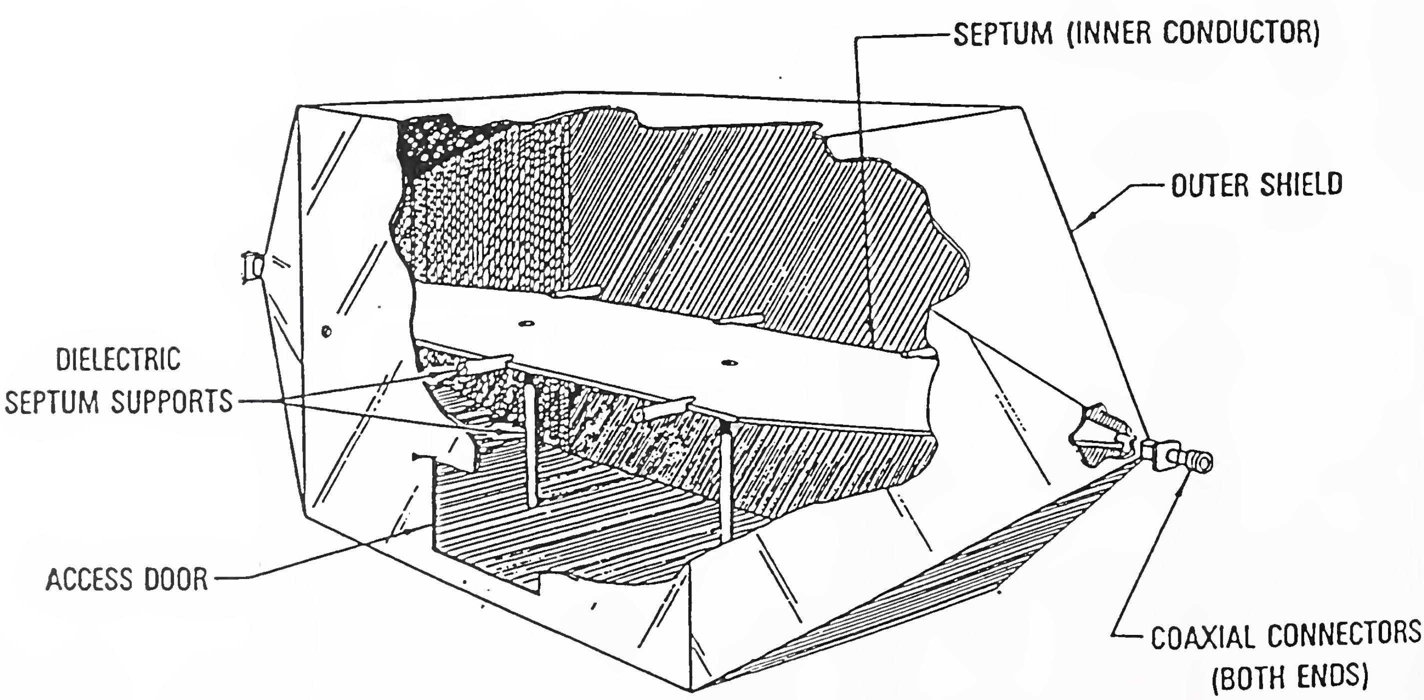

Figure 1. Geometry for a TEM cell.

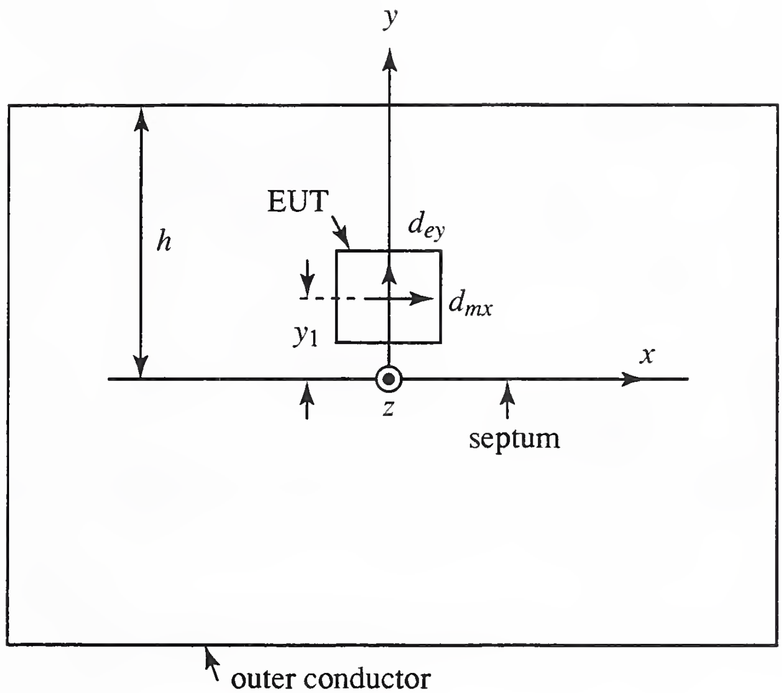

Figure 2. Cross-sectional view of an EUT with electric and magnetic dipole moments located above the septum in a TEM cell.

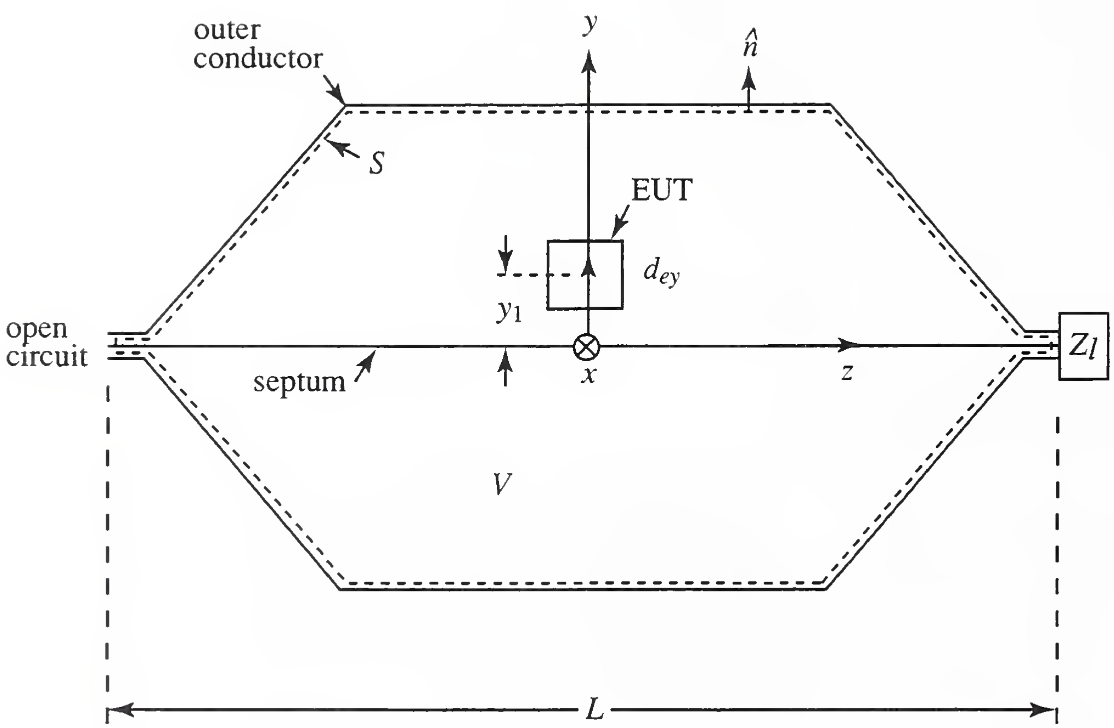

Figure 3. Side view of an EUT located above the septum in an open-circuited TEM cell.

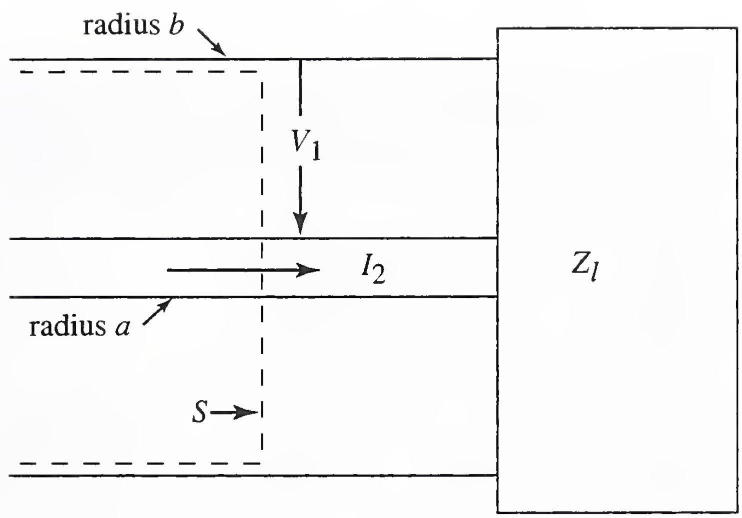

Figure 4. Impedance termination of the coaxial section of a TEM cell.

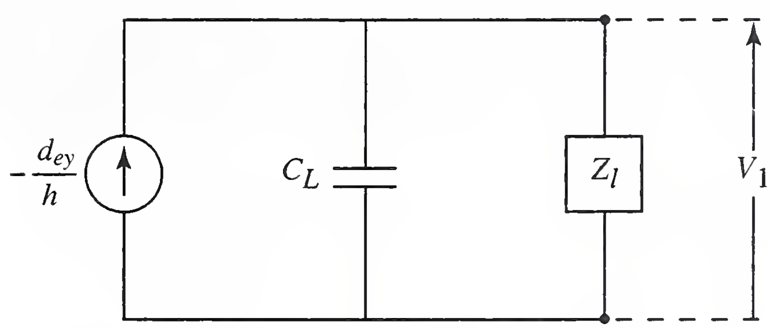

Figure 5. Equivalent circuit for an electric dipole source in an open-circuited TEM cell.

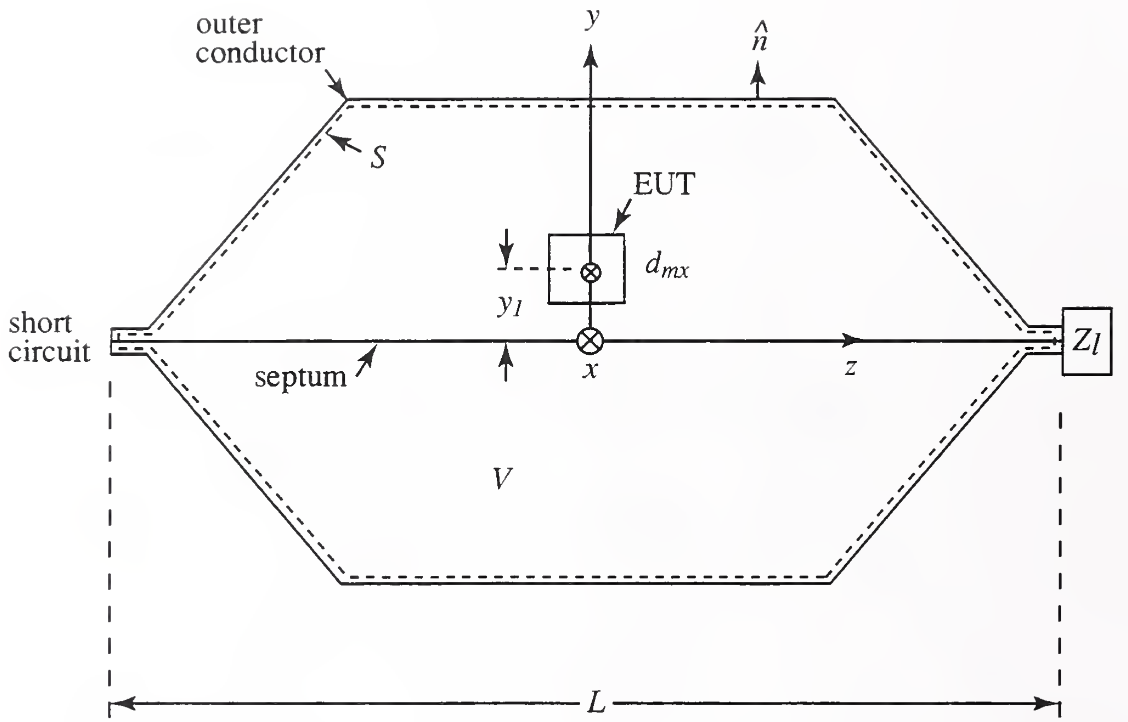

Figure 6. Side view of an EUT located above the septum in a short-circuited TEM cell.

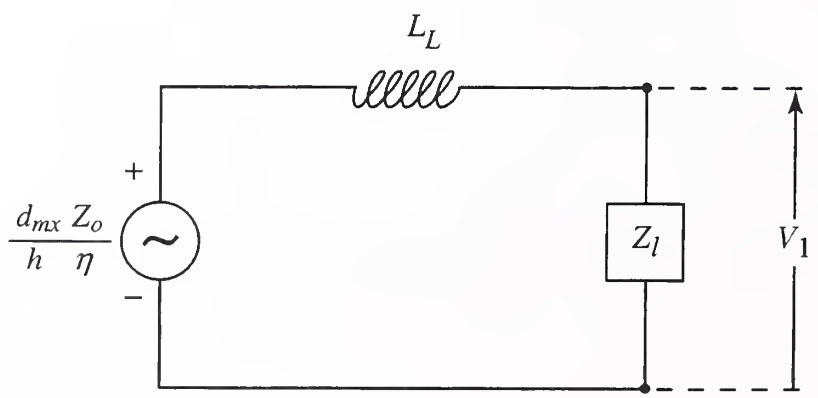

Figure 7. Equivalent circuit for a magnetic dipole source in a short-circuited TEM cell.

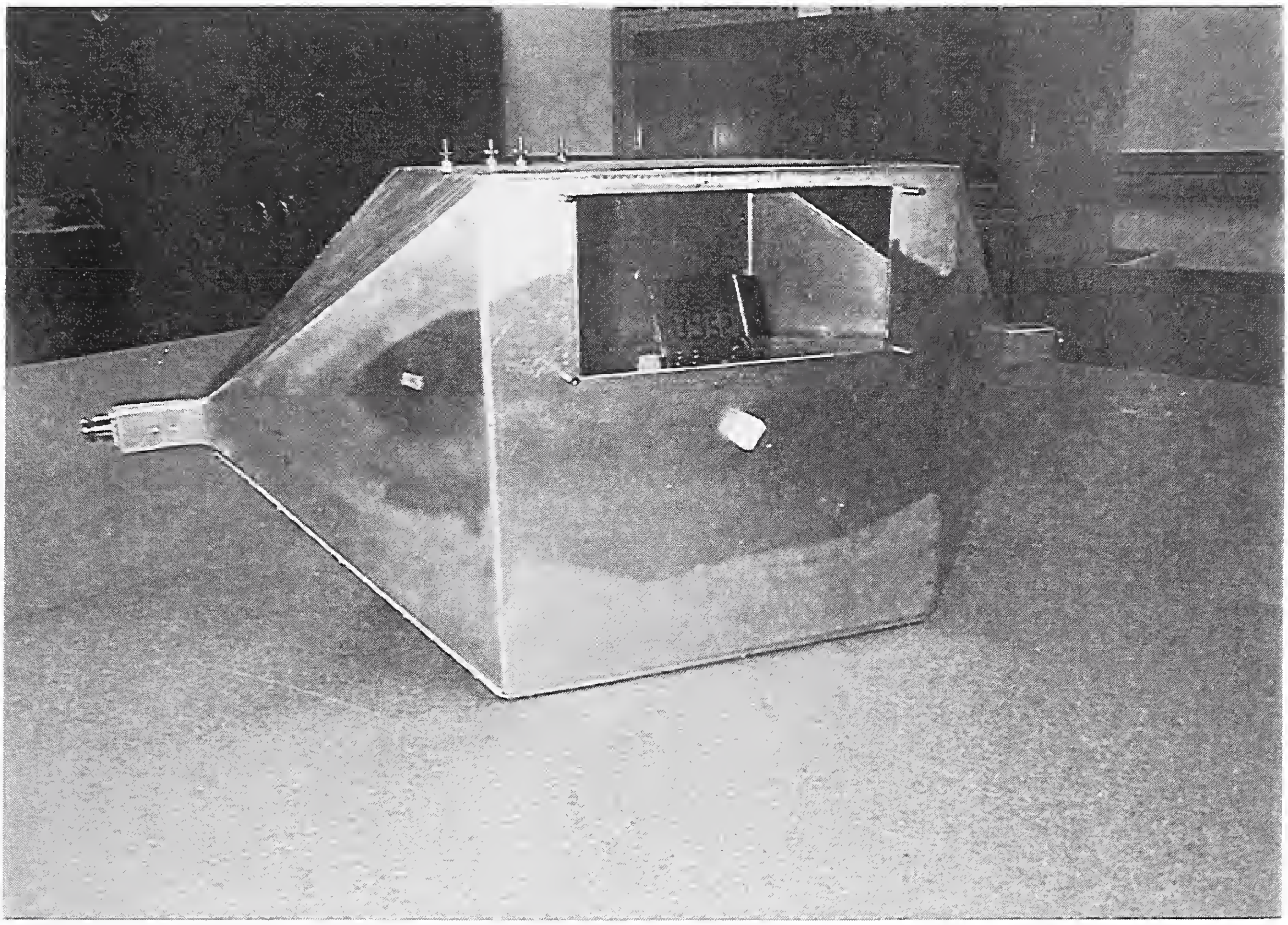

Figure 8. Photograph of an electronic timer in a TEM cell.

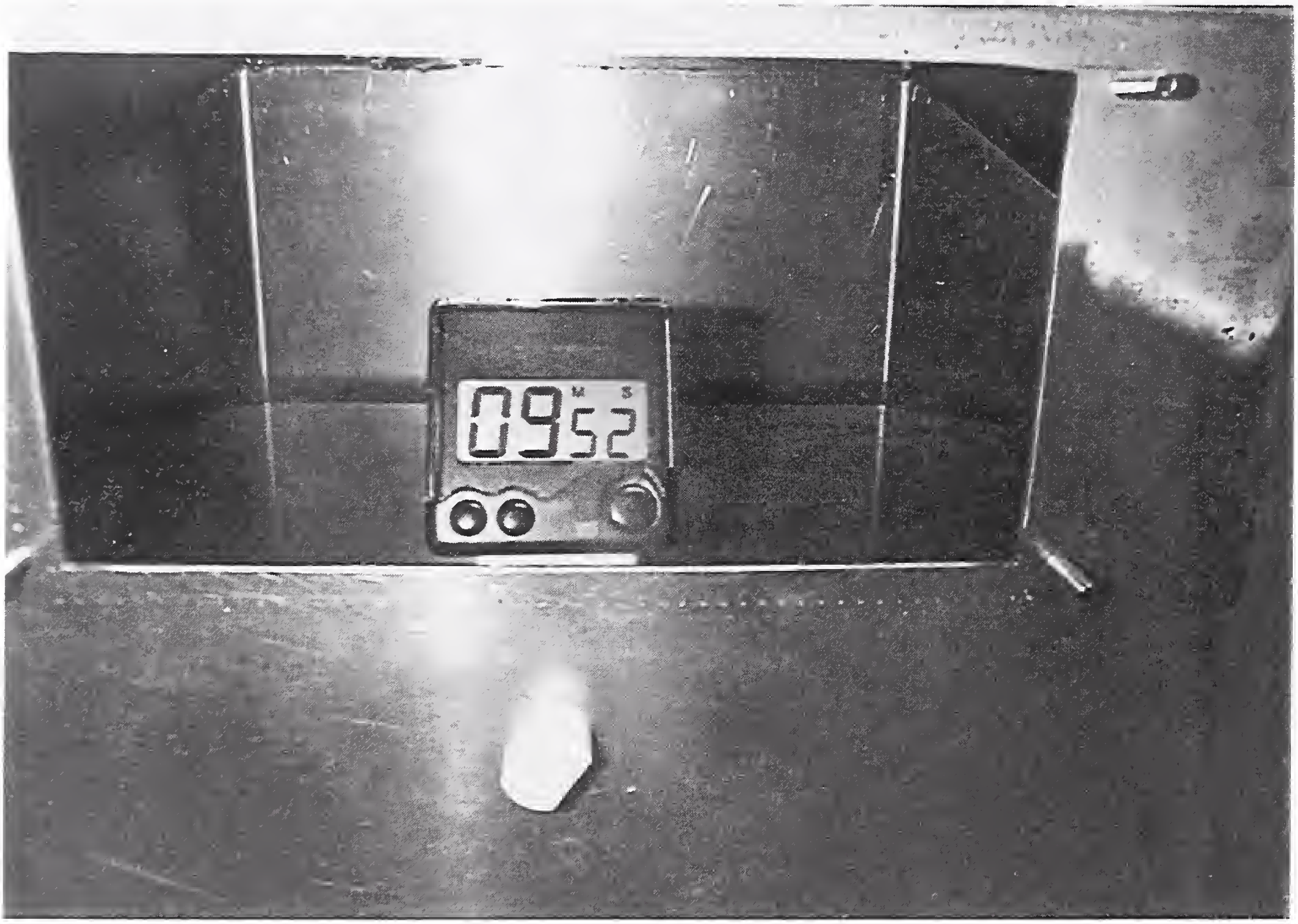

Figure 9. Closeup photograph of an electronic timer in a TEM cell.

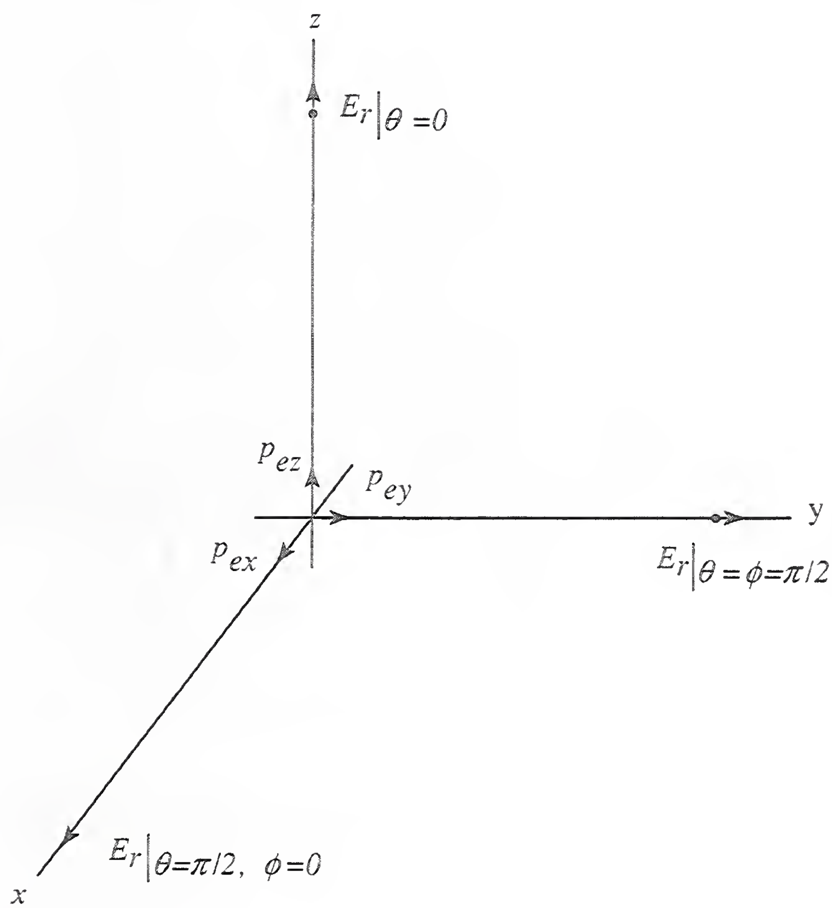

Figure 10. Geometry for electric dipoles at the origin and radial electric fields on the axes.

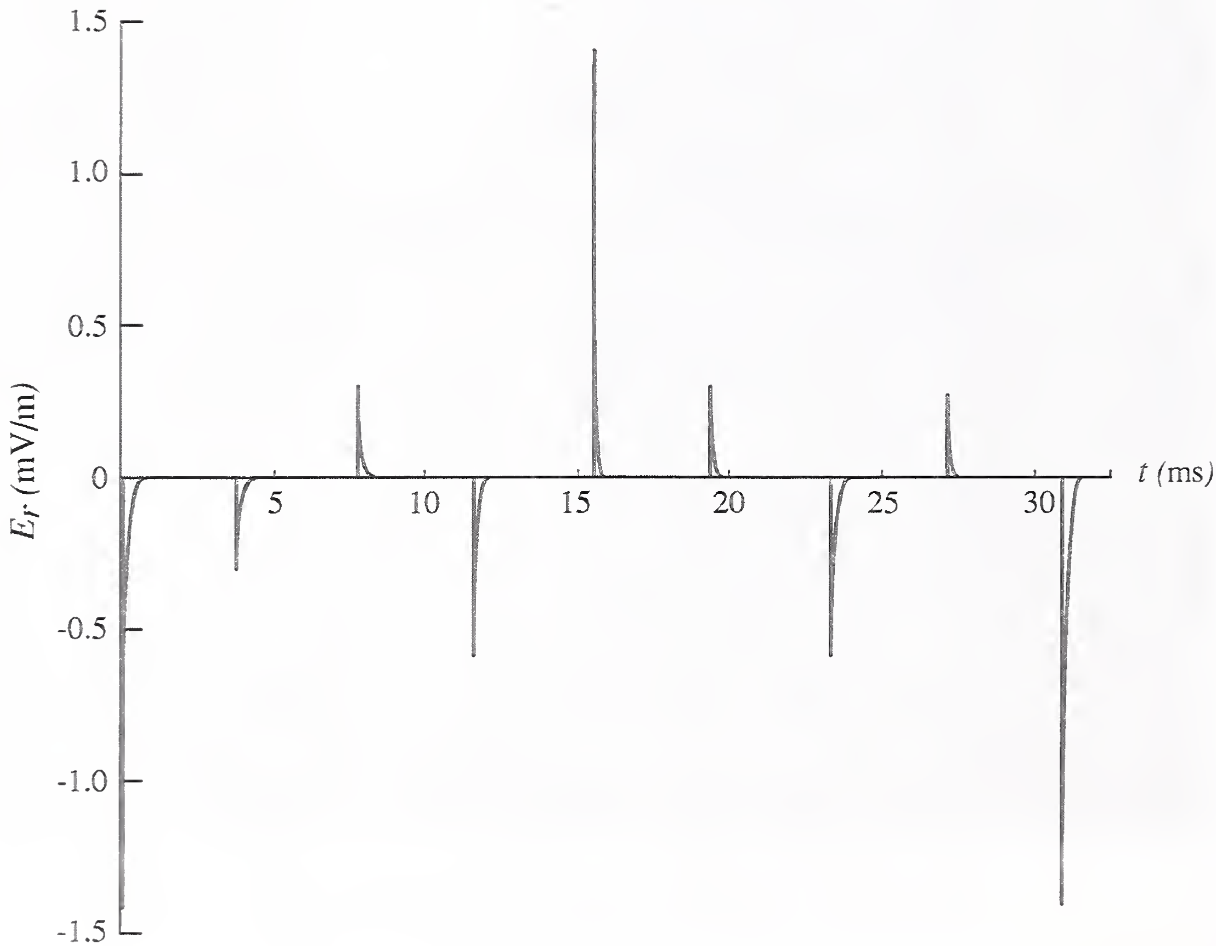

Figure 11. Time-domain waveform for the radial electric field at 1 m from an electronic timer.

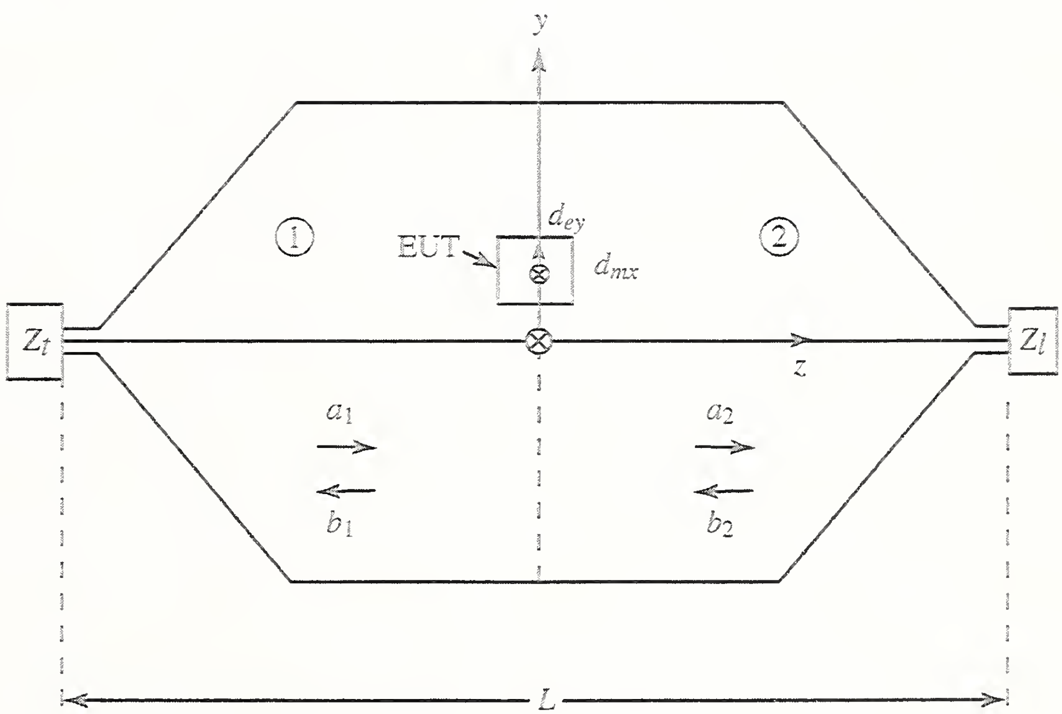

Figure 12. Side view of an EUT located in a TEM cell with arbitrary terminations.